

# Constructing and Evaluating an Explainable Model for COVID-19 Diagnosis from Chest X-rays

**Rishab Khincha**

*BITS Pilani, Goa, India*

F20160517@GOA.BITS-PILANI.AC.IN

**Soundarya Krishnan**

*BITS Pilani, Goa, India*

F20160472@GOA.BITS-PILANI.AC.IN

**Krishnan Guru-Murthy**

*West Middlesex University Hospital - NHS, Middlesex, UK*

KGMURTHY33@GMAIL.COM

**Tirtharaj Dash**

*BITS Pilani, Goa, India*

TIRTHARAJ@GOA.BITS-PILANI.AC.IN

**Lovekesh Vig**

*TCS Research, New Delhi, India*

LOVEKESH.VIG@TCS.COM

**Ashwin Srinivasan**

*BITS Pilani, Goa, India*

ASHWIN@GOA.BITS-PILANI.AC.IN

## Abstract

In this paper, our focus is on constructing models to assist a clinician in the diagnosis of COVID-19 patients in situations where it is easier and cheaper to obtain X-ray data than to obtain high-quality images like those from CT scans. Deep neural networks have repeatedly been shown to be capable of constructing highly predictive models for disease detection directly from image data. However, their use in assisting clinicians has repeatedly hit a stumbling block, because of their black-box nature. Some of this difficulty can be alleviated if predictions were accompanied by explanations expressed in clinically-relevant terms. In this paper, deep neural networks are used to extract domain-specific features (morphological features like ground glass opacity and disease indications like pneumonia) directly from the image data. Predictions about these features are then used to construct a symbolic model (a decision tree) for the diagnosis of COVID-19 from chest X-rays. We accompany

these predictions with two kinds of explanations: visual (saliency maps, derived from the neural stage), and textual (logical descriptions, derived from the symbolic stage). A radiologist rates the usefulness of the visual and textual explanations. Our results suggest that: (a) There is no significant loss in predictive accuracies when using the neural-symbolic model over using a single end-to-end model; and (b) The radiologist usually finds at least one of visual or textual explanations relevant; In addition, the textual explanations are better than a “textual baseline” more often than the corresponding visual case. This suggests either: the textual representation is more relevant to the diagnostic task, or that the visual representation is not very relevant for the diagnostic task, or both. Taken together, these results demonstrate that neural models can be employed usefully in identifying domain-specific features from low-level image data; that textual explanations in terms of clinically-relevant features may be useful; and

that visual explanations will need to be clinically meaningful to be useful.

**Keywords:** Hybrid models, Neural-Symbolic models, Human-in-the-loop, Explainable ML, COVID-19

## 1. Introduction

The use of explainable symbolic models for diagnosis of disease is not new (MYCIN and Internist-I, for example, were developed from the early 1970s, with just this purpose Shortliffe and Buchanan (1975); Miller et al. (1982)). Neither is the use of hierarchical approaches to Computer Vision, in which high-level symbolic models use the results of low-level feature-extraction from raw images (see for example, Ballard and Brown (1982)). For most of these, the symbolic component has fulfilled purpose of generating limited answers to “Why” type questions. Recent developments in hardware, storage, and algorithmic optimisation has however made possible the construction of very large end-to-end neural network models that are capable of predicting the probability of disease, directly from raw image data (see Fig. 1)

Although end-to-end models can produce accurate diagnosis of COVID-19 (Asnaoui and Chawki, 2020; Toğaçar et al., 2020; Mangal et al., 2020; Wang and Wong, 2020; Gozes et al., 2020), they are often considered as black-box models, with little or no explanatory power (Lipton, 2016). This has proved to be a stumbling block in their clinical acceptability.

However, interpretability and explainability of these models has not been a focus for these works. Work in these areas is crucial for acceptance by physicians, as well as for sanity checks during model development.

Saliency-like visual explanations (GSInquire in Wang and Wong (2020) and Grad-CAMs in Mangal et al. (2020); Karim et al. (2020) have been used to highlight the rel-

evant regions for the diagnosis made by the model. However, these maps may have less utility in a medical setting, consistent to previous findings like in Arun et al. (2020). None of these works explore any other means of explanations. Most crucially, most works do not consult clinicians to find out which types of explanations are actually meaningful to them and assist them in diagnosis.

In this paper, we investigate the use of a hierarchical neural-symbolic approach for COVID-19 diagnosis, accompanied by a description of why the diagnosis was reached. We consider two kinds of explanations: (a) Visual, in the form of saliency maps from the neural-stage that construct the domain-specific features used for diagnosis; and (b) Textual, in the form of a description obtained from the symbolic model when making a diagnosis. We compare these against the following baselines that are agnostic to any decision being made: (c) A simple segmentation map of the lungs; and (d) A simple tabulation of the input to the symbolic model for the data instance being diagnosed. The thinking here is that for (a) to be a relevant visual explanation, it should be judged (by a radiologist) to be at least better than (c); and for (b) to be relevant, it should be judged (again, by a radiologist) to be at least better than (d).

Recently, a categorisation of model explainability has been proposed by Arrieta et al. (2019). In this categorisation, explanations in (a) constitute local, visual explanations; and (b) constitute global, textual explanations. To promote reproducibility of our findings, and for any future extensions, we provide the datasets collected from an experienced radiologist on request.

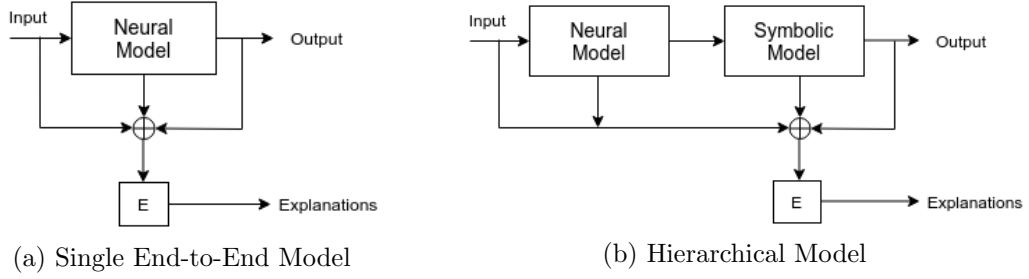


Figure 1: Two approaches to building explainable models

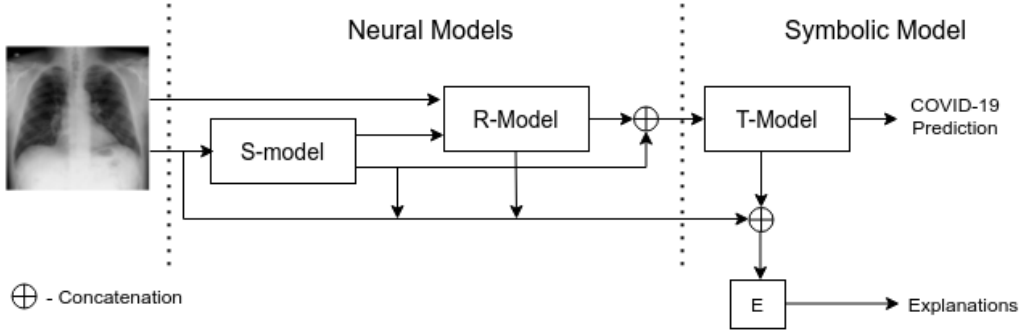


Figure 2: Neural-Symbolic Pipeline for COVID-19 diagnosis. The *S*-model is a deep network for predicting symptoms; the *R*-model is a deep network for predicting radiological features; and the *T*-model is a decision-tree. *E* refers to a set of procedures for extracting visual and symbolic explanations.

## 2. Neural-Symbolic Modelling for Diagnosis and Explanation

In this section, we describe a hierarchical approach for obtaining diagnoses and explanations. The first stage of the hierarchical approach performs a form of domain-specific representation-learning. Two deep neural networks are used to obtain clinically relevant features directly from images. The *S*-model is a deep network that predicts symptomatic features like consolidations, pleural effusions and so on. The *R*-model is a deep network that predicts morphological features like ground-glass opacity and air-space opacifications (see Fig. 2). The principal datasets used in each of the models are shown in Table 1.

### 2.1. Stage 1: Neural Models for Clinical Features

The *S*-model is a CheXNet (Rajpurkar et al., 2017) model, obtained by minimising the binary crossentropy loss using an Adam optimizer.

The *R*-model is a deep model that identifies radiologically-relevant morphological symptoms. The model in this paper focuses on predicting the occurrence of various forms of opacification in chest X-rays. To train the *R*-model, we use a dataset assembled from: (a) Morphological annotations for COVID-19 X-rays from the COVIDx dataset - we call this the COVIDr dataset; (b) Images for pneumonia patients taken from the NIH dataset; (c) Images for healthy and tuberculosis patients taken from the Pulmonary Chest X-ray dataset. The COVIDr dataset

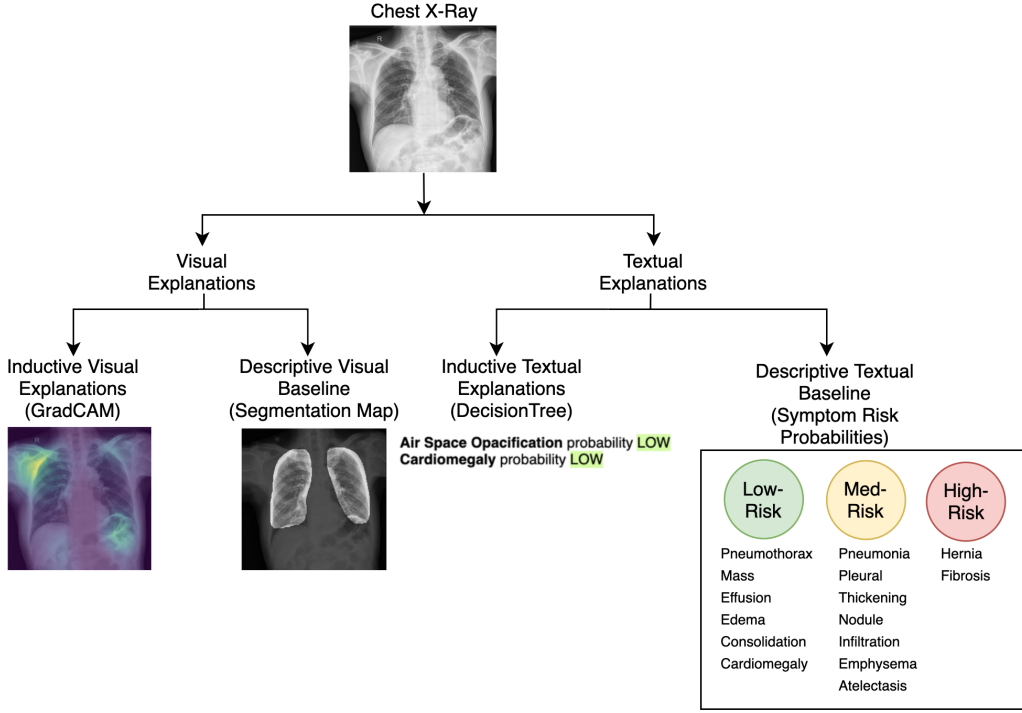


Figure 3: Explanations for COVID-19 diagnosis

contains annotations made by one of the co-authors (a practising radiologist). We describe the annotation process first.

Chest X-rays from COVID-19 positive patients are annotated with one of 7 morphological labels. Here, we are interested in simply two broad categories of these labels, namely the presence (or absence) of Ground Glass Opacity (*GGO*) and Air Space Opacification (*ASO*). In COVID-19 images, *GGO* is *present* if the Ground Glass Opacity annotation is marked as present; and *ASO* is *present* if any of: Bilateral or Unilateral Air Space Opacification annotations are marked as *present* (See Appendix A for more details on the COVIDr dataset). For healthy samples, we assume both *GGO* and *ASO* are absent. For tuberculosis and pneumonia patients, both *GGO* and *ASO* are not known (these images were not seen during annotation).

The *R*-model is constructed to predict a 1-hot encoding of one of 5 values: only *GGO* is *present*; only *ASO* is *present*; both *GGO* and *ASO* are *present*; both *GGO* and *ASO* are *absent*; and both *GGO* and *ASO* are unknown. The model is constructed using a training, validation, and the independent held-out test data as described Section 3.3. Input data for constructing the model consist of chest X-ray images, and the predictions of the *S*-model. The final model is obtained by minimising the categorical cross-entropy loss using an Adam optimizer.

## 2.2. Stage 2: Symbolic Model for Diagnosis

In this stage, outputs of the *S* and *R*-models along with labels for images are used to construct a decision-tree for COVID-19 diagnosis (the class-labels for the decision-tree are *COV+* or *COV-*, where the latter refers to

Table 1: Datasets Table

Dataset	Model	Details
NIH Chest X-ray <a href="#">Wang et al. (2017)</a>	<i>S</i> -model	112,120 X-ray images with 14 disease labels from 30,805 unique patients. Default train-val-test split used.
	<i>R</i> -model	Pneumonia images used. Train(234) and test(88).
Pulmonary Chest X-ray <a href="#">Jaeger et al. (2014)</a>	<i>Seg</i> -model	Chest X-rays and their masks used. Train (566) and Test (134)
	<i>R</i> -model	Tuberculosis and healthy Chest X-rays used. Tuberculosis - Train (295) and Test (88); Healthy - Train(294) and Test(110)
COVIDx <a href="#">Cohen et al. (2020)</a>	<i>Seg</i> -model	Chest X-rays and their manually annotated masks used.
	<i>R</i> -model	COVID-19 positive Chest X-rays used. Train (196) and Test (30)
COVIDr	<i>R</i> -model	Relevant radiological annotations from one of our co-authors(a practicing radiologist) for COVID-19 positive Chest X-rays from COVIDx. See Appendix A for details.

images of healthy, pneumonia and tuberculosis patients).<sup>1</sup> Details of tree-construction are in Section 3.3.

### 2.3. Explanations

We examine two kinds of model-based explanations visual and textual, each with the corresponding baselines. We use the term “inductive” to qualify the explanation based on a machine-constructed model. The baselines are simple summarisations of the relevant features of the data, and are qualified by the term “descriptive”. We require the inductive explanations to be at least as use-

ful to the clinicians as the descriptive summaries. Details of these categories are:

**Visual, Inductive.** This consists of class activation maps (GradCAMs, proposed by [Selvaraju et al. \(2016\)](#)), showing gradations of saliency in the *R*-model.

**Visual, Descriptive.** This acts of a baseline for the corresponding inductive explanation. It consists of masks showing a segmentation of the lungs obtained using a deep network.

**Symbolic, Inductive.** This is a translation of the sequence of decisions made by the symbolic model in reaching a diagnosis.<sup>2</sup>

1. The input to for tree-construction are probability vectors for symptoms and boolean-values for the morphological features. Recall the *R*-models essentially predict whether *GGO* and *ASO* are present, absent, or missing.

2. For simplicity, we leave out statements about missing values when generating explanations. It is unclear whether statements of the form “X

**Symbolic, Descriptive.** This acts as a baseline for assessing the utility of the corresponding inductive explanation. It is a tabulation of discretised values of probabilities of the outputs of the  $S$  and  $R$ -models. The discretisation is into 3 simple categories (*high*, *medium*, and *low*).

Examples of each of these kinds of these categories are shown in Fig. 3.

### 3. Empirical Evaluation

#### 3.1. Aims

Our aim is to test the neural-symbolic system proposed in Section 2 along the following dimensions:

- **Predictive** We investigate if there is any significant loss in predictive accuracy over using a single end-to-end deep network model with access to the same image data.
- **Explanatory** We investigate the clinical usefulness of the visual and symbolic explanations described earlier.

#### 3.2. Materials

##### 3.2.1. DATA

The datasets used in this paper are shown in Table 1. The COVIDr dataset has been annotated by one of our co-authors, who is a practising radiologist. It captures important ground glass opacities and air space opacifications from the Chest X-rays relevant to the diagnosis of COVID-19 (See Appendix A for more details).

---

is missing” are of value to the radiologist, but such an expression can nevertheless have predictive value.

##### 3.2.2. ALGORITHMS AND MACHINES

All the experiments are conducted in Python environment (Tensorflow/Keras) in a machine with 64GB main memory, 16-core Intel processor and 8GB NVIDIA P4000 graphics processor.

#### 3.3. Methods

We adopt the following method for evaluation of predictive accuracy:

1. Split the COVIDx dataset into *COVIDxTrain* and *COVIDxTest*
2. Construct an end-to-end deep model on the *COVIDxTrain* data and use it to obtain predictions on the *COVIDxTest* data.
3. Construct an  $S$ -model using the *NIH* dataset and use it to obtain predictions for the *COVIDxTrain* data.
4. Construct an  $R$ -model using pre-trained weights (see details below), and the *COVIDxTrain* data and use it to construct predictions for morphological features for the *COVIDxTrain* data.
5. Construct a  $T$ -model (decision tree) using the outputs of the  $S$ -model (Step 3) and the  $R$ -model (Step 4) and use it to obtain predictions on the *COVIDxTest* data
6. Compare the estimated accuracies on *COVIDxTest* of the  $T$ -model (Step 5) and the end-to-end deep model (Step 2)

The following details are relevant:

- We use the default split provided by Cohen et al. (2020) for splitting the COVIDx data in *COVIDxTrain* and the completely held out test-set, *COVIDxTest*

- Pre-trained weights for the end-to-end model are from ImageNet. The learning rate used was  $10^{-4}$  and the model was trained for 500 epochs.
- The train, validation and test set for the *S*-model uses the default split from Wang et al. (2017) with 62428, 6336, and 1518 images respectively.
- There are two choices for pre-trained weights for the *R*-model. We have a choice of either using a generic pre-training (using ImageNet) or the domain-specific pre-training (using the end-to-end model in Step 2). We use a subset of *COVIDxTrain* as a validation set to decide between these alternatives, which resulted in the use of domain-specific pre-trained weights.
- We split the *COVIDxTrain* set into a 85-15 train-val set to construct the *R*-model. We perform a sweep across 3 learning rate settings ( $10^{-3}$ ,  $10^{-4}$  and  $10^{-5}$ ) and epochs (100, 250, 500) and the train split to build 9 *R*-models. The one performing best on the val split is selected as our final *R*-model.
- Assessments of comparative difference in accuracies are made using a Gaussian approximation to the Binomial distribution. Given an accuracy of  $p$  on *COVIDxTest*, the standard deviation (s.d) is given by  $\sqrt{p(1-p)/n}$ , where  $n$  is the number of instances in *COVIDxTest*. Then a difference in accuracy is taken to be significant if it is 2 or more s.d's away.

We adopt the following method for evaluation of explanations. For a subset of images in *COVIDxTest*:

1. Obtain inductive visual and textual explanations along with their correspond-

ing baselines. explanations (inductive and descriptive)

2. Obtain a radiological assessment of (a) Utility of visual and textual explanations; (b) Comparative utility of visual and textual explanations with the baselines.

The following details are relevant:

- Visual inductive explanations are class activation maps obtained using Grad-CAM. Visual descriptive baselines are obtained using the lung segmentation model trained in Section 2.3.
- Textual descriptive baselines are obtained from the predictions of the *R* and the *S*-models by binning the probabilities into *Low* ( $\leq 0.33$ ), *Medium* ( $\leq 0.67$ ) or *High*.
- The radiological assessments of the utility for each of the individual explanations as well as the comparative utilities are obtained by asking the radiologist a series of questions described in Appendix C.

### 3.4. Results

The main observations to note are these:<sup>3</sup> (1) The estimated predictive accuracy of the end-to-end approach is  $0.985 \pm 0.007$  and that of the Neural-Symbolic approach is  $0.973 \pm 0.009$  (Table 2); (2) Visual explanations are marked as relevant on 21/30 instances. Of these, in 5/21 instances the inductive explanation is marked as being more useful than the corresponding descriptive baseline (see Table 4a); (3) Textual explanations are marked as relevant on 18/30 instances. Of these, in 13/18 instances the inductive explanation is marked as being more useful than

---

3. Here, we term an explanation as “relevant” if it is *useful* or *somewhat useful*.



Table 2: Confusion Matrices for COVID-19 Prediction. (COV+ is COVID-19 positive; COV− is not COVID-19 positive)

(a) End to End model				(b) Neural-Symbolic Model			
Act \ Pred	Pred			Act \ Pred	Pred		
	COV+	COV−			COV+	COV−	
COV+	26	4		COV+	23	7	
COV−	1	297		COV−	2	296	

Table 3: Usefulness of explanations and baselines as rated by the radiologist (Vis-Visual; Text-Textual; Ind-Inductive; Des-Descriptive)

	Vis-Ind	Vis-Des	Text-Ind	Text-Des
Useful	14	21	17	6
Somewhat Useful	7	5	1	4
Not Useful	9	1	12	20

that the corresponding descriptive baseline (see Table 4b); (4) Either one of visual or textual explanation is marked as relevant in 29/30 instances. (See Table 3 for details about the utility of each of the representations we provide.

**[Explanations are Useful.]** Either visual or textual explanations were considered radiologically relevant in 29/30 instances. This suggests that it could be useful to augment clinical diagnoses with such additional information.

**[Domain-Specific Representations are Important.]** There seems to be a reversal in preference from the descriptive baseline to the inductive explanation when going from visual to textual explanations. This is against a backdrop of a high frequency of preference for visual representations (21/30 instances). We believe several factors to be involved here. First, radiological diagnosis is largely image-based. This results in a natural preference for visual representations. However, the fact that the baseline of a simple lung segmentation is

preferred over the saliency maps suggests that the latter do not correspond in any meaningful way. This is not the case with textual explanations that use radiologically meaningful features: hence the greater preference for the inductive explanation over the tabulation of descriptive statistics. Taken together, the results highlight the need to construct explanations in clinically meaningful terms. This supports a finding by Arun et al. (2020) that direct presentation of GradCAM visualisation may not be ‘trustworthy’, or relevant in a medical context.

**[“Simpler” Explanations are Preferable.]** We think the apparent preference for visual baseline and textual inductive explanations over the visual inductive explanation also indicate an underlying preference for simpler explanations. The visual baseline is simply a delineation of the lungs; and the preferred inductive textual explanation is a small set of conditions leading to the diagnosis. In contrast, the saliency maps and tabulations of probabilities contains



Table 4: Conditional comparison of inductive explanations ( $I$ ) and descriptive baseline ( $D$ ). ( $X > Y$  means that  $X$  is more useful than  $Y$ )

(a) Comparison given Visual Explanations (V) are relevant.

	Count
$I > D$	5
$I < D$	8
$I = D$	8

(b) Comparison given Textual Explanations (T) are relevant.

	Count
$I > D$	13
$I < D$	0
$I = D$	5

Table 5: Agreements between the model (M) and the radiologist (R) when the latter is sure

	M	Agree	Disagree
R			
Sure		19	6

Table 6: Correct and Incorrect predictions of the model (M) when the radiologist (R) is unsure

	M	Correct	Incorrect
R			
Unsure		4	1

significantly more detail, most of which is probably not thought to be clinically relevant. While the lung-segmentation image does not constitute any kind of explanation for the diagnosis of the model, it is not entirely irrelevant, since radiologists do look at lung-appearance during diagnosis.

**[Models Can Assist.]** Our results in Tables 5 and 6 suggest that the model is not simply a clone of the radiologist, and could be helpful in cases where the diagnosis is not clear-cut. This opens up the possibility of using such systems as a second opinion when making diagnoses.

#### 4. Concluding Remarks

In this paper, we have examined the use of a hierarchical neural-symbolic approach for diagnosis of COVID-19 from chest X-rays. Our findings suggest that it is possible to construct hierarchical models with accuracies comparable to end-to-end models, with

additional benefits arising the ability to construct visual and textual explanations using the neural and symbolic stages of the approach. We have also presented some evidence of an assessment of these explanations. Specifically, we find that while explanations are relevant, they are better than a simple “baseline explanation” only for the symbolic explanation that is a simple logical description using domain-specific concepts. This does not mean visual explanations are not meaningful: rather that the specific use of saliency maps is not useful.

A focus on explanations and keeping the clinician-in-the-loop is crucial for deployment of models as clinical assistants, so that clinicians gain trust in the decision of these machines, and possibly make better judgments. The deployment of quick and reliable model-based tools is becoming increasingly important in the context of COVID-19, as it threatens to overwhelm medical practitioners in countries with limited medical expertise.

It has been repeatedly shown in machine learning, that accuracy of models depends

crucially on the representation used, and that the acceptance of machine-learned models depends crucially on whether the models are able to capture meaningful mechanisms. Future work in this area needs to focus therefore on the domain-specific features to identify automatically from image-data, and how to develop convey the concepts identified to the radiologists in a manner in which they can assess clinical significance. We think this can only be achieved by a continuous dialogue between clinicians and developers of machine-learning models.

## References

- Alejandro Barredo Arrieta, Natalia Díaz-Rodríguez, Javier Del Ser, Adrien Benetot, Siham Tabik, Alberto Barbado, Salvador García, Sergio Gil-López, Daniel Molina, Richard Benjamins, Raja Chatila, and Francisco Herrera. Explainable artificial intelligence (xai): Concepts, taxonomies, opportunities and challenges toward responsible ai, 2019.
- Nishanth Arun, Nathan Gaw, Praveer Singh, Ken Chang, Mehak Aggarwal, Bryan Chen, Katharina Hoebel, Sharut Gupta, Jay Patel, Mishka Gidwani, Julius Adebayo, Matthew D. Li, and Jayashree Kalpathy-Cramer. Assessing the (un)trustworthiness of saliency maps for localizing abnormalities in medical imaging, 2020.
- Khalid El Asnaoui and Youness Chawki. Using x-ray images and deep learning for automated detection of coronavirus disease. *Journal of Biomolecular Structure and Dynamics*, 0(0):1–12, 2020. URL <https://doi.org/10.1080/07391102.2020.1767212>.
- Dana Harry Ballard and Christopher M. Brown. *Computer Vision*. Prentice Hall Professional Technical Reference, 1st edition, 1982. ISBN 0131653164.
- Joseph Paul Cohen, Paul Morrison, Lan Dao, Karsten Roth, Tim Q Duong, and Marzyeh Ghassemi. Covid-19 image data collection: Prospective predictions are the future, 2020.
- Ophir Gozes, Maayan Frid-Adar, Hayit Greenspan, Patrick D. Browning, Huangqi Zhang, Wenbin Ji, Adam Bernheim, and Eliot Siegel. Rapid ai development cycle for the coronavirus (covid-19) pandemic: Initial results for automated detection & patient monitoring using deep learning ct image analysis, 2020.
- Stefan Jaeger, Sema Candemir, Sameer Antani, Yi-Xiáng Wáng, Pu-Xuan Lu, and George Thoma. Two public chest x-ray datasets for computer-aided screening of pulmonary diseases. *Quantitative imaging in medicine and surgery*, 4:475–7, 12 2014. doi: 10.3978/j.issn.2223-4292.2014.11.20.
- Md. Rezaul Karim, Till Döhmen, Dietrich Rebholz-Schuhmann, Stefan Decker, Michael Cochez, and Oya Beyan. Deepcovidexplainer: Explainable covid-19 diagnosis based on chest x-ray images, 2020.
- Zachary Chase Lipton. The mythos of model interpretability. *CoRR*, abs/1606.03490, 2016. URL <http://arxiv.org/abs/1606.03490>.
- Arpan Mangal, Surya Kalia, Harish Rajgopal, Krithika Rangarajan, Vinay Namboodiri, Subhashis Banerjee, and Chetan Arora. Covidaid: Covid-19 detection using chest x-ray, 2020.
- Randolph A. Miller, Harry E. Pople, and Jack D. Myers. Internist-i, an experimental computer-based diagnostic consultant for general internal medicine. *New England Journal of Medicine*, 307(8):468–476, 1982. doi: 10.1056/NEJM198208193070803. URL <https://doi.org/10.1056/NEJM198208193070803>. PMID: 7048091.
- Pranav Rajpurkar, Jeremy Irvin, Kaylie Zhu, Brandon Yang, Hershel Mehta, Tony Duan, Daisy Ding, Aarti Bagul, Curtis Langlotz, Katie Shpanskaya, Matthew P. Lungren, and Andrew Y. Ng. Chexnet: Radiologist-level pneumonia detection on chest x-rays with deep learning, 2017.
- Ramprasaath R. Selvaraju, Abhishek Das, Ramakrishna Vedantam, Michael

- Cogswell, Devi Parikh, and Dhruv Batra. Grad-cam: Why did you say that? visual explanations from deep networks via gradient-based localization. *CoRR*, abs/1610.02391, 2016. URL <http://arxiv.org/abs/1610.02391>.
- Edward H. Shortliffe and Bruce G. Buchanan. A model of inexact reasoning in medicine. *Mathematical Biosciences*, 23(3):351 – 379, 1975. ISSN 0025-5564. doi: [https://doi.org/10.1016/0025-5564\(75\)90047-4](https://doi.org/10.1016/0025-5564(75)90047-4). URL <http://www.sciencedirect.com/science/article/pii/0025556475900474>.
- Mesut Toğaçar, Burhan Ergen, and Zafer Cömert. Covid-19 detection using deep learning models to exploit social mimic optimization and structured chest x-ray images using fuzzy color and stacking approaches. *Computers in Biology and Medicine*, 121:103805, 2020. ISSN 0010-4825. URL <http://www.sciencedirect.com/science/article/pii/S0010482520301736>.
- Linda Wang and Alexander Wong. Covid-net: A tailored deep convolutional neural network design for detection of covid-19 cases from chest x-ray images, 2020.
- Xiaosong Wang, Yifan Peng, Le Lu, Zhiyong Lu, Mohammadhadi Bagheri, and Ronald Summers. Chestx-ray8: Hospital-scale chest x-ray database and benchmarks on weakly-supervised classification and localization of common thorax diseases. *arXiv:1705.02315*, 05 2017.

## Appendix A. COVIDr Dataset

The details of the COVIDr dataset are seen in Table 7. An example of the way we parse the dataset is shown in Fig. 4.

## Appendix B. Model Details

The *R*- and *S*-Model architectures are shown in Fig. 5. Details of conversion of the Neural Radiology Model (*R*-model) output to Symbolic Tree (*T*-model) input are shown in Table 8.

To check for the optimal maximum leaf nodes, we plot (Fig. 6a) the test accuracy against the number of leaf nodes. We also try to find the optimal maximum depth of the tree, as shown in Fig. 6b.

The tree obtained from the Symbolic model that is described in Section 1 is shown in Fig. 7. The extracted rules are shown below.

### Rules for COVID-Positive

1.  $P(ASO) > 0.5$
2.  $P(ASO) \leq 0.5$   
 $\&\& P(\text{Missing GGO}/ASO) \leq 0.5$   
 $\&\& P(\text{Infiltration}) > 0.406$   
 $\&\& P(\text{Emphysema}) \leq 0.122$
3.  $P(ASO) \leq 0.5$   
 $\&\& P(\text{Missing GGO}/ASO) \leq 0.5$   
 $\&\& P(\text{Infiltration}) \leq 0.406$   
 $\&\& P(\text{Emphysema}) > 0.127$   
 $\&\& P(\text{Edema}) > 0.085$

### Rules for COVID-Negative

1.  $P(ASO) \leq 0.5$   
 $\&\& P(\text{Missing GGO}/ASO) \leq 0.5$
2.  $P(ASO) \leq 0.5$   
 $\&\& P(\text{Missing GGO}/ASO) \leq 0.5$   
 $\&\& P(\text{Infiltration}) > 0.406$   
 $\&\& P(\text{Emphysema}) > 0.122$   
 $\&\& P(\text{Emphysema}) \leq 0.122$

3.  $P(ASO) \leq 0.5$   
 $\&\& P(\text{Missing GGO}/ASO) \leq 0.5$   
 $\&\& P(\text{Infiltration}) \leq 0.406$   
 $\&\& P(\text{Emphysema}) > 0.127$   
 $\&\& P(\text{Edema}) \leq 0.085$
4.  $P(ASO) \leq 0.5$   
 $\&\& P(\text{Missing GGO}/ASO) \leq 0.5$   
 $\&\& P(\text{Infiltration}) \leq 0.406$   
 $\&\& P(\text{Emphysema}) \leq 0.127$

## Appendix C. Web-Based interface for collecting feedback

One of our co-authors, who is also a practising radiologist, provides utility assessments for 30 Chest X-ray images sampled from the held-out test set (COVID-19 positive - 5, healthy - 5, tuberculosis - 5 and pneumonia - 5), along with the COVID-19 diagnosis made by our model and all the explanations as stated in Section 2.3. We provide a web-based interface and ask the following questions in the given order :

1. Prior to revealing the diagnosis of a given Chest X-ray image made by the model (true label is never revealed) or the corresponding explanations, we ask for the radiologist's diagnosis. We then reveal the diagnosis made by the model.
2. We ask the radiologist to rate the visual quality of the image as Low, Medium or High.
3. The visual explanations (*VisInd*, *VisDed*) provided by our model are then displayed side by side along with the Chest X-ray. We then ask if each of these explanations individually are *Useful*, *Somewhat Useful* or *Not Useful*. We also ask whether the *VisInd* explanations was more useful, *VisDed* explanations was more useful or if both are the same.

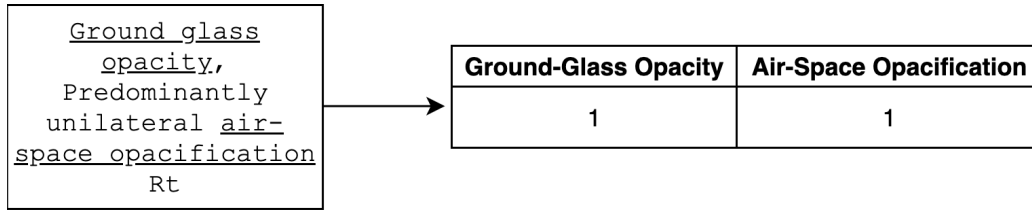


Figure 4: Parsing the COVIDr dataset

Table 7: The COVIDr dataset consists of 7 CXR finding labels for COVID-19 positive images. The number of positive instances of these labels are shown in the accompanying table.

CXR-Finding	Positive Instances
None	44/245 (17.95%)
Ground glass opacity	145/245 (59.18%)
Bilateral patchy air-space opacification	30/245 (12.24%)
Bilateral symmetrical air-space opacification	18/245 (7.34%)
Bilateral peripheral air-space opacification	54/245 (22.04%)
Predominantly unilateral air-space opacification Rt	36/245 (14.69%)
Predominantly unilateral air-space opacification Lt	28/245 (11.4%)

Table 8: Conversion of Neural Radiology Model output to Symbolic Tree input

Max Prob.	ASO	GGO
ASO	1	0
GGO	0	1
ASO_GGO	1	1
No_ASO_GGO	0	0
Missing_ASO_GGO	?	?

- The symbolic explanations(*SymInd*, *SymDed*) provided by our model are displayed side by side along with the Chest X-ray. We then ask if each of these explanations individually are *Useful*, *Somewhat Useful* or *Not Useful*. We also ask whether the *SymInd* explanations was more useful, *SymDed* explanations was more useful or if both are the same.

- Finally, we ask which explanations were more useful - Visual, Symbolic or both were the same.

Snippets of the web interface are shown in Fig. 8

## Appendix D. Additional Results

### D.1. COVIDr Baselines

We benchmark the COVIDr dataset by training different variation to predict the morphological symptoms. The results are shown in Table 9.

### D.2. Symbolic Model Baselines

The results of our symbolic model are shown in Table 10. We compare these results with a single end-to-end, as well as other tree-based models. We find that the loss in accuracy in our symbolic model is not significant in comparison with the black box model,

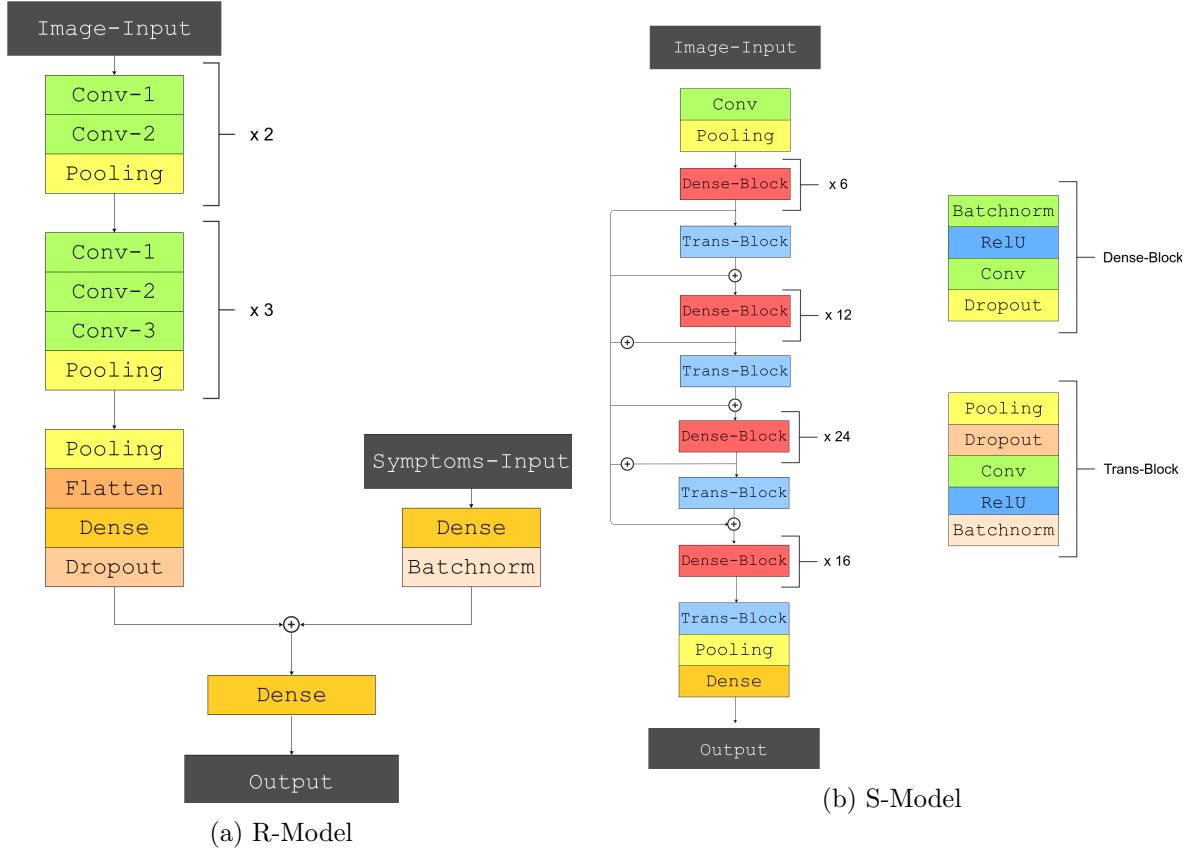


Figure 5: Neural model architectures

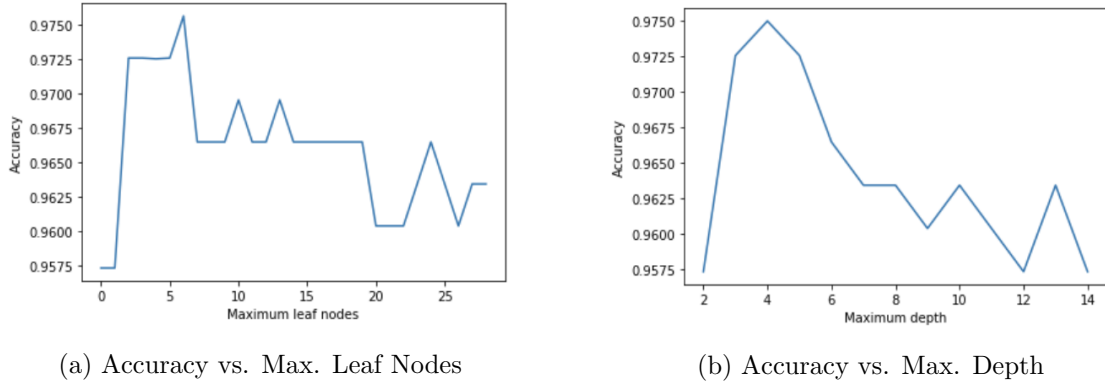


Figure 6: Optimal Leaf Nodes and Depth

and the tree model additionally provides interpretable explanations. We also see that our decision tree has very similar predictive

power as with other tree ensembling methods like *Random Forest* and *XGBOOST*.



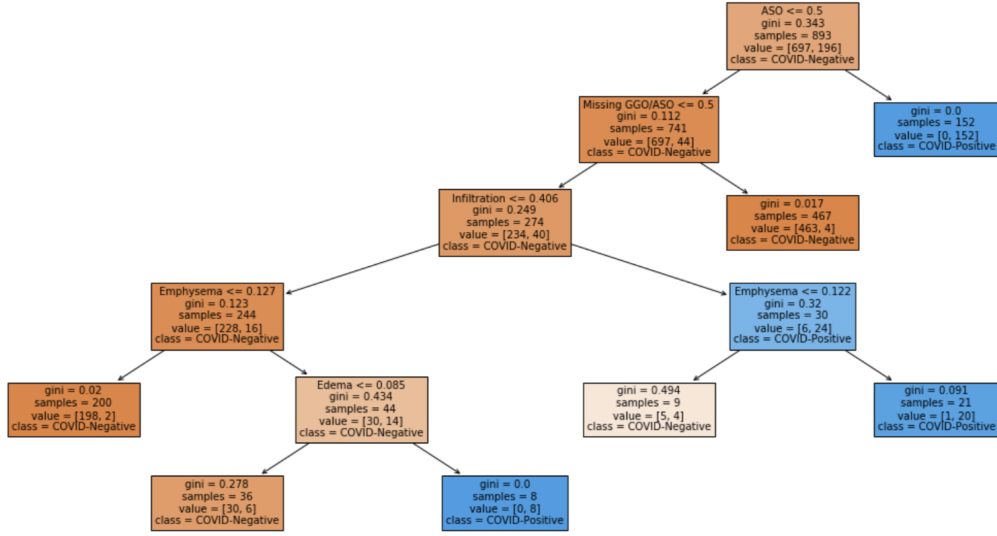


Figure 7: Tree used to generate textual inductive explanations

Table 9: Results on the Radiology Model.  
 (Sym– Model using embeddings from the  $S$ -model. PT– VGG16 uses pre-trained weights from the end-to-end model)

Model	Accuracy	AUC
VGG-16	0.83	0.96
VGG-16 + Sym	0.86	0.97
VGG-16 + Sym (PT)	<b>0.88</b>	<b>0.99</b>

Table 10: Results on the COVID-19 prediction

Model	Accuracy	F1
End-to-End	<b>0.985 <math>\pm</math> 0.007</b>	<b>0.95</b>
NS-RF	0.973 $\pm$ 0.009	0.915
NS-XGB	0.973 $\pm$ 0.009	0.930
NS-DTree	0.973 $\pm$ 0.009	0.915

## EXPLAINABLE MODELS FOR COVID-19

Click on the button for any image to go to our explainabl diagnoses

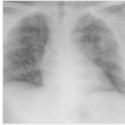


Image 1

Go to Step 2: Diagnose




Image 2

Go to Step 2: Diagnose




Image 3

Go to Step 2: Diagnose




Image 4

Go to Step 2: Diagnose




Image 6

### Your diagnosis

0

Your Diagnosis \*

- ☐ COVID
- ☐ Non-COVID
- ☐ Unsure

What do you think is the quality of this image? \*

- ☐ Average to Low Quality
- ☐ High Quality



Submit Diagnosis

Show AI Diagnosis

### PART 1: Visual Explanations

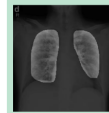
1 Inductive Visual Saliency Maps

These are the areas that our model focused on while making the prediction

2 Descriptive Visual Segmentation Maps

These are the lung regions isolated by our model



Legend

Low Importance High Importance

### PART 2: Textual Explanations

1 Inductive Textual

These are the symptoms detected as present or not present by our machine learning model. These are the symptoms that helped our system make its decision

Air Space Opacification probability **88%**

2 Descriptive Textual

These are the symptoms along with the probabilities detected by our system

Low Prob	Med Prob	High Prob
Asymptomatic	Presymptomatic	Healthy Person
Common Cold	Flu	
COVID-19		

### Feedback for Visual Explanations

0

Feedback for Saliency Maps (Left)

☐ Helpful ☐ Somewhat helpful ☐ Not helpful

Feedback for Segmentation Maps (Right)

☐ Helpful ☐ Somewhat helpful ☐ Not helpful

Which among Saliency Maps and Segmentation Maps is better?

☐ Saliency Maps are better ☐ Both are same ☐ Segmentation Maps are better

Submit Feedback

### Feedback for Textual Explanations

0

Feedback for Decision Tree Path (Left)

☐ Helpful ☐ Somewhat helpful ☐ Not helpful

Feedback for Descriptive Statistics (Right)

☐ Helpful ☐ Somewhat helpful ☐ Not helpful

Which among Symptoms Found and Symptoms Risks is better?

☐ Symptoms Found are better ☐ Both are same ☐ Symptoms Risks are better

Submit Feedback

### Overall Feedback

Which among Visual Explanations and Textual Explanations is better?

☐ Visual Explanations are better ☐ Both are same ☐ Textual Explanations are better

Do you want to change your diagnosis? If yes, please select your diagnosis.

☐ COVID ☐ Non-COVID ☐ Unsure

Submit Feedback

Go to the next image

Figure 8: Snippet of Interface that the Radiologist uses to evaluate explanations and base-lines